

Lattice Boltzmann electrokinetics simulation of nanocapacitors

Cite as: *J. Chem. Phys.* **151**, 114104 (2019); doi: [10.1063/1.5119341](https://doi.org/10.1063/1.5119341)

Submitted: 11 July 2019 • Accepted: 28 August 2019 •

Published Online: 16 September 2019



View Online



Export Citation



CrossMark

Adelchi J. Asta,¹ Ivan Palaia,² Emmanuel Trizac,² Maximilien Levesque,³  and Benjamin Rotenberg^{1,4,a} 

AFFILIATIONS

¹Sorbonne Universités, CNRS, Physico-Chimie des électrolytes et Nanosystèmes Interfaciaux, F-75005 Paris, France

²LPTMS, UMR 8626, CNRS, Univ. Paris-Sud, Université Paris-Saclay, 91405 Orsay, France

³PASTEUR, Département de Chimie, École Normale Supérieure, PSL University, Sorbonne Université, CNRS, 75005 Paris, France

⁴Réseau sur le Stockage Electrochimique de l'Énergie (RS2E), FR CNRS 3459, Amiens, France

^aElectronic mail: benjamin.rotenberg@sorbonne-universite.fr

ABSTRACT

We propose a method to model metallic surfaces in Lattice Boltzmann Electrokinetics (LBE) simulations, a lattice-based algorithm rooted in kinetic theory which captures the coupled solvent and ion dynamics in electrolyte solutions. This is achieved by a simple rule to impose electrostatic boundary conditions in a consistent way with the location of the hydrodynamic interface for stick boundary conditions. The proposed method also provides the local charge induced on the electrode by the instantaneous distribution of ions under voltage. We validate it in the low voltage regime by comparison with analytical results in two model nanocapacitors: parallel plates and coaxial electrodes. We examine the steady-state ionic concentrations and electric potential profiles (and corresponding capacitance), the time-dependent response of the charge on the electrodes, and the steady-state electro-osmotic profiles in the presence of an additional, tangential electric field. The LBE method further provides the time-dependence of these quantities, as illustrated on the electro-osmotic response. While we do not consider this case in the present work, which focuses on the validation of the method, the latter readily applies to large voltages between the electrodes, as well as to time-dependent voltages. This work opens the way to the LBE simulation of more complex systems involving electrodes and metallic surfaces, such as sensing devices based on nanofluidic channels and nanotubes, or porous electrodes.

Published under license by AIP Publishing. <https://doi.org/10.1063/1.5119341>

I. INTRODUCTION

Interfaces between metals and electrolyte solutions play the central role in electrochemistry as well as in many analytical chemistry techniques. Electrodes are also necessary to apply an electric field to manipulate charged objects in solutions, such as colloidal particles or electrolytes. As a result, electrode-electrolyte interfaces have been extensively studied both experimentally and theoretically over a century. Recent technological advances have made it possible to design experimental setups in which electrolyte solutions are confined between electrodes separated by very small distances, down to a few tens or hundreds of nanometers, or within carbon nanotubes which may also exhibit partially metallic behavior.¹ The ability to build such nanocapacitors opens the way to new analytical strategies based on electrochemistry with a very limited number of redox-active species, using nanofluidic devices^{2–4}

or thin layer cells,⁵ and questions our basic understanding of coupled fluid and charge flows, or electrokinetic phenomena, through single nanotubes.^{6–9}

Significant progress has been made in the understanding of the electric double layer (EDL) at charged or metallic interfaces since the pioneering Gouy-Chapman-Stern theory.^{10–12} In recent years, simulations have become a powerful tool to predict their structure and dynamics without the need to rely on strong simplifying assumptions, which are generally required to obtain analytical theoretical results. For example, Brownian dynamics simulations allowed to investigate the relaxation of the EDL after a charge transfer event,¹³ treating the metallic electrodes as homogeneously charged surfaces and the solvent as a dielectric continuum. At the atomistic level, the introduction of models allowing to perform molecular simulation of electrodes maintained at a constant potential (as in a perfect metal), rather than constant charge,^{14,15} opened the way to detailed

investigations of electrochemical interfaces. These studies showed the importance of taking the polarization of the metal by the electrolyte into account.^{16–19} However, the computational cost of such atomistic simulations restricts their use to small systems (below 10 nm) and relatively concentrated electrolytes (due to the small number of ions in such small volumes).

The dynamics of ions in the bulk and in EDLs, and in turn the charging dynamics of nanocapacitors, results from their thermal motion (diffusion) and their migration due to the local electric field they experience. Taking these factors into account allows us to provide a detailed description of the charging dynamics in capacitors in planar^{20,21} or more complex (e.g., porous) geometries.²² Another process by which ions move is their advection by the local fluid flow, which may vanish by symmetry in some simple cases, but cannot be neglected *a priori*. Together with the fluid flow induced by the net local charge within the EDL, this is at the origin of the above-mentioned electrokinetic phenomena, which have been long studied theoretically or numerically with simulations, from molecular^{23–25} to models with various levels of coarse-graining (see, e.g., Refs. 26 and 27 for reviews on multiscale simulation approaches).

Among these mesoscopic simulation approaches for electrokinetics (such as dissipative particle dynamics²⁸ or multiparticle collision dynamics^{29,30}), Lattice Boltzmann³¹ (LB) has emerged as an efficient compromise between the simplicity of the solvent description, based on kinetic theory and allowing to recover proper hydrodynamic behavior and on the flexibility with which it can be coupled to explicit particles or free energy models to describe complex fluids. In the former case, Molecular Dynamics (MD) coupled to LB was successfully used to investigate the electrokinetic effects with charged colloids,^{32,33} polyelectrolytes in the bulk³⁴ or grafted on surfaces³⁵ or their translocation through nanopores,³⁶ and more recently (and closer to the subject of the present work) to the response of EDLs to changes in the charge of surfaces.³⁷

The other approach, where no explicit particles are present, exists in different flavors, which can broadly be seen as efficient numerical solvers of the continuous electrokinetic equations, even though their roots on kinetic theory also provide additional information on the dynamics of species. In that respect, treating solvent and ions on the same footing in a multicomponent LB model³⁸ is a promising approach to capture correlations, in particular, due to the discrete nature of solvent molecules and ions at this coarse-grained level, especially under extreme confinement (comparable to molecular sizes). For larger systems, the LB method is rather coupled to numerical schemes to describe the evolution of ions. Assuming their instantaneous relaxation (on the time scale over which the fluid evolves) toward the Poisson-Boltzmann equilibrium, for charged³⁹ or constant-potential⁴⁰ walls, does not allow investigating the relaxation of the ionic concentration and potential profiles in the EDLs. This requires an explicit integration of the ionic dynamics, typically solving the Nernst-Planck equation (described below), via finite difference/element methods. This has, for example, been used to simulate electrokinetic effects in porous media^{41,42} or electrochemical desalination.⁴³ Numerical schemes to solve the Nernst-Planck equation using the structure of the Lattice Boltzmann algorithm have also been proposed, which introduce a fictitious dynamics for the electrostatic potential to solve the Poisson equation.^{44–46}

An alternative hybrid approach for the dynamics of ions coupled to the LB method for that of the fluid makes consistent use of the LB lattice. Inspired by previous work based on the moment propagation method⁴⁷ and extending a previous attempt with ionic fluxes computed on the lattice node,⁴⁸ Capuani *et al.* proposed a method focusing instead on the ionic fluxes through each link connecting nodes of the lattice (via the discrete lattice velocities).⁴⁹ This point of view has a number of advantages, such as strictly enforcing charge conservation, in particular, at solid-liquid boundaries, and offering a statistical interpretation which can be exploited to compute other properties such as velocity auto-correlation functions via moment propagation.⁵⁰ This hybrid LB/link-flux method, called Lattice Boltzmann Electrokinetics (LBE), has been successfully used to investigate the dynamics of charged colloids,^{51–55} charged porous media and ions in oil-water mixtures,⁵⁶ or binary colloidal suspensions.⁵⁷ In these systems, electrostatic boundary conditions at solid-liquid interfaces correspond to constant charge (Neumann, i.e., constant normal electric field), rather than constant potential (Dirichlet).

In the present work, we show that a simple rule to impose Dirichlet electrostatic boundary conditions allows the simulation of systems involving metallic surfaces using LBE simulations. Specifically, the method leads to imposing the target potential at the location of the hydrodynamic interface, i.e., between the solid and liquid nodes rather than solely on the solid nodes. In addition, it is possible to determine the instantaneous local charge on the electrode at virtually no additional cost. This opens the way to the simulation of the dynamic response of electric double layers in capacitors by following the evolution of the ionic concentrations and potential profiles as well as the charge of the electrodes. The LBE method also naturally captures the electrokinetic couplings with the solvent. The proposed implementation of electrostatic boundary conditions is readily applicable to arbitrary electrode geometries, just as the bounce-back rule to impose no-slip boundary conditions.

The electrokinetic equations and the LBE algorithm are presented in Sec. II, together with the proposed method to impose constant-potential boundary conditions and to compute the charge induced on the (blocking) electrode by the instantaneous distribution of ions under voltage. We then demonstrate the validity of the method in Sec. III by considering capacitors in two geometries, parallel plates and coaxial electrodes, in the regime of small applied voltage, for which analytical results are available [Debye-Hückel (DH) theory for the ionic concentration and electric potential profiles, together with Stokes for the steady-state electro-osmotic profiles]. We also show numerical results for the transient regime for electro-osmosis in the presence of an additional, tangential electric field, for which no analytical results are available. While we do not consider this case in the present work, which focuses on the validation of the method, the latter readily applies to large voltages between the electrodes.

II. METHOD

A. Electrokinetic equations

The canonical description of electrokinetic couplings in a dilute electrolyte consisting of k ionic species with valencies z_k and

diffusion coefficients D_k in a solvent characterized by its mass density ρ , dynamic viscosity η , and dielectric permittivity $\epsilon_0\epsilon_r$ couples the Poisson-Nernst-Planck equations for the dynamics of ions and the Navier-Stokes equation for that of the solvent. The Nernst-Planck equation is a conservation equation for the ionic concentrations ρ_k ,

$$\frac{\partial \rho_k}{\partial t} + \nabla \cdot [\rho_k \mathbf{u} + \mathbf{j}_k] = \frac{\partial \rho_k}{\partial t} + \nabla \cdot [\rho_k \mathbf{u} - D_k \nabla \rho_k - \beta D_k z_k e \rho_k \nabla \psi] = 0, \quad (1)$$

where $\beta = 1/k_B T$ with k_B being the Boltzmann constant and T being the temperature, e is the elementary charge, \mathbf{u} is the local velocity of the fluid and where the electrostatic potential ψ satisfies the Poisson equation

$$\nabla^2 \psi = -\frac{1}{\epsilon_0 \epsilon_r} \rho_{el} = -\frac{e}{\epsilon_0 \epsilon_r} \sum_k \rho_k z_k. \quad (2)$$

The three terms in the flux defined by Eq. (1) correspond to advection, diffusion, and migration under the effect of the local electric field $-\nabla \psi$, respectively. The advective part depends on the local velocity \mathbf{u} which is assumed to satisfy the Navier-Stokes equation for an incompressible fluid ($\nabla \cdot \mathbf{u} = 0$),

$$\rho \left(\frac{\partial \mathbf{u}}{\partial t} + (\mathbf{u} \cdot \nabla) \mathbf{u} \right) = \eta \nabla^2 \mathbf{u} - \sum_k \rho_k \nabla \mu_k + \mathbf{f}_V^{ext}, \quad (3)$$

with \mathbf{f}_V^{ext} being the external force density and the chemical potentials $\mu_k = \mu_k^{id} + \mu_k^{ex} = k_B T \ln(\rho_k/\rho_k^0) + z_k e \psi$ include an ideal part (with ρ_k^0 being a reference concentration) and an excess part assumed to arise only from mean-field electrostatic interactions. The excess part results, together with the applied electric field \mathbf{E}_{app} when present, in a local electric force acting on the fluid $e(\sum_k z_k \rho_k)(-\nabla \psi + \mathbf{E}_{app})$ in Eq. (3).

These coupled equations should be solved for prescribed boundary conditions at solid-liquid interfaces, usually stick (no-slip) for hydrodynamics ($\mathbf{u} = 0$) and Neumann (constant field, corresponding to a fixed surface charge density) or Dirichlet (constant potential) for electrostatics.

At equilibrium, the ionic fluxes and fluid velocities vanish. From Eq. (1), the concentration profiles then follow Boltzmann distributions $\rho_k = \rho_k^0 e^{-z_k \beta e \psi}$. From Eq. (2), the potential satisfies the Poisson-Boltzmann equation

$$\nabla^2 \psi = -\frac{e}{\epsilon_0 \epsilon_r} \sum_k \rho_k^0 z_k e^{-z_k \beta e \psi}, \quad (4)$$

which can be linearized for small potentials (Debye-Hückel limit) as

$$\nabla^2 \psi = \kappa^2 \psi = \frac{1}{\lambda_D^2} \psi, \quad (5)$$

with the Debye screening length

$$\lambda_D = \kappa^{-1} = \left(4\pi l_B \sum_k \rho_k^0 z_k^2 \right)^{-1/2}, \quad (6)$$

where the Bjerrum length $l_B = \frac{\beta e^2}{4\pi \epsilon_0 \epsilon_r}$ is the distance at which the Coulomb interaction between two unit charges is equal to the thermal energy ($l_B = 0.7$ nm in water at room temperature, which

corresponds to all the simulation results shown in the rest of this work).

B. Lattice Boltzmann electrokinetics

The Lattice Boltzmann Electrokinetics (LBE) algorithm is a hybrid lattice scheme coupling the standard Lattice Boltzmann (LB) method for the dynamics of the fluid, which captures, in particular, overall mass and momentum conservation, with the link-flux method for the evolution of its composition, in particular, the diffusion, advection, and migration of the ions. Since its introduction by Capuani *et al.*,⁴⁹ it has been used and described many times and we only recall the basics to focus on the novelty of the present work, which is the introduction of new electrostatic boundary conditions described in Sec. II C.

The LB method can be derived as a discretized version of a continuous kinetic equation for the evolution of the probability density function $f(\mathbf{r}, \mathbf{v}, t)$ to find a fluid particle with a velocity \mathbf{v} at position \mathbf{r} at time t . The moments of f in the velocity space provide the hydrodynamic observables, such as the local density $\rho(\mathbf{r}, t) = \int f(\mathbf{r}, \mathbf{v}, t) d\mathbf{v}$, local mass flux $\rho(\mathbf{r}, t) \mathbf{u}(\mathbf{r}, t) = \int f(\mathbf{r}, \mathbf{v}, t) \mathbf{v} d\mathbf{v}$, and local stress tensor. The Boltzmann equation with the Bhatnagar-Gross-Krook (BGK) collision operator is discretized consistently in space (cubic grid with lattice spacing Δx), time (with time step Δt), and velocity space with a finite set of velocities $\{\mathbf{c}_i\}$ with associated populations $f_i(\mathbf{r}, t) \equiv f(\mathbf{r}, \mathbf{c}_i, t)$ and weights w_i . Here, we use the three-dimensional D3Q19 lattice,³¹ with 19 velocities corresponding to 0, nearest, and next-nearest neighbors (with respective norms 0, $\frac{\Delta x}{\Delta t}$, and $\sqrt{2} \frac{\Delta x}{\Delta t}$ and weights $\frac{1}{3}$, $\frac{1}{18}$, and $\frac{1}{36}$), and a lattice speed unit related to the thermal velocity $c_s^2 = \frac{k_B T}{m} = \frac{1}{3} \left(\frac{\Delta x}{\Delta t} \right)^2$, with m being the mass of the fluid particles.

The local hydrodynamic variables are computed exactly from the populations as

$$\rho(\mathbf{r}, t) = \sum_i w_i f_i(\mathbf{r}, t); \quad \rho \mathbf{u}(\mathbf{r}, t) = \sum_i w_i f_i(\mathbf{r}, t) \mathbf{c}_i \quad (7)$$

and the populations evolved according to

$$f_i(\mathbf{r} + \mathbf{c}_i \Delta t, t + \Delta t) = f_i(\mathbf{r}, t) - \frac{\Delta t}{\tau} [f_i(\mathbf{r}, t) - f_i^{eq}(\mathbf{r}, t)] + F_i(\mathbf{r}, t), \quad (8)$$

where τ is the characteristic time for the relaxation toward the local Maxwell-Boltzmann distribution f_i^{eq} and controls the viscosity of the fluid, while $F_i(\mathbf{r}, t)$ accounts for the effect of local force density. The latter includes external forces as well as the internal contribution of local chemical potential gradients [see Eq. (3)]. To ensure numerical stability and accuracy of the algorithm, the fluid velocity must remain small compared to the speed of sound c_s of the LB fluid. This small Mach number condition then implies “sufficiently small” volumic forces f_V , i.e., $\chi_T f_V \Delta x \ll 1$, with χ_T being the fluid compressibility ($\chi_T = 1/\rho c_s^2$ for the LB fluid). The choice of the lattice spacing will be further discussed in Sec. II C.

The ionic concentrations are discretized on the same spatial grid and time steps and evolved using the link-flux method, separating the contribution of advection from the ones arising from the ideal and excess chemical potential gradients, as described in Ref. 49 to which we refer the reader for the advection part. The

contributions of chemical potential gradients are expressed in a symmetrized form by writing the fluxes $\mathbf{j}_k = -D_k e^{-\beta\mu_k^{\text{ex}}} \nabla[\rho_k e^{+\beta\mu_k^{\text{ex}}}]$. This leads to the update of the amount of solutes on each node, $n_k(\mathbf{r}, t) = \rho_k(\mathbf{r}, t)\Delta x^3$, according to

$$n_k(\mathbf{r}, t + \Delta t) - n_k(\mathbf{r}, t) = -A_0 \sum_i j_k^i(\mathbf{r}, t), \quad (9)$$

where the sum runs over discrete velocities, j_k^i is the contribution of each link between \mathbf{r} and $\mathbf{r} + \mathbf{c}_i \Delta t$ to the flux of species k through the cell boundary around node \mathbf{r} , and A_0 is a lattice-dependent geometric factor (equal to $1 + 2\sqrt{2}$ for D3Q19). The link-fluxes are given by

$$j_k^i(\mathbf{r}, t) = -d_k \frac{e^{-\beta\mu_k^{\text{ex}}(\mathbf{r})} + e^{-\beta\mu_k^{\text{ex}}(\mathbf{r} + \mathbf{c}_i \Delta t)}}{2} \times \left[\frac{n_k(\mathbf{r} + \mathbf{c}_i \Delta t) e^{+\beta\mu_k^{\text{ex}}(\mathbf{r} + \mathbf{c}_i \Delta t)} - n_k(\mathbf{r}) e^{+\beta\mu_k^{\text{ex}}(\mathbf{r})}}{\Delta_i} \right] \quad (10)$$

with $d_k = (D_k/A_0)/(\Delta x^2/\Delta t)$ and $\Delta_i = \|\mathbf{c}_i\|/(\Delta x/\Delta t)$. While this choice of discretization leads to spurious fluxes when the lattice spacing is too large (large potential differences between neighboring nodes),⁵⁴ this form enforces that the ionic concentrations follow the Boltzmann distribution at equilibrium.

At each time step, the excess chemical potentials are computed from the local electrostatic potential determined from the ionic concentrations by solving numerically the Poisson equation as described in Sec. II C. The effect of thermodynamic forces, arising from the local excess chemical potential gradients, on the dynamics of the fluid [see Eq. (3)] is expressed from the link-fluxes, in dimensionless units, via the term

$$F_i(\mathbf{r}, t) = -\frac{c_s^2}{(\Delta x/\Delta t)^2} \sum_k \left[\frac{j_k^i(\mathbf{r}, t)}{d_k} - \frac{n_k(\mathbf{r} + \mathbf{c}_i \Delta t) - n_k(\mathbf{r})}{\Delta_i} \right] \quad (11)$$

in Eq. (8).

No-slip hydrodynamic boundary conditions are enforced by the bounce-back rule, which places the interface at the midplane between liquid and solid nodes³¹ while setting the link-fluxes to zero through the corresponding links ensures the absence of leakage of ions inside the solid. Together with the advection of ions (see Ref. 49 for more details), the link-flux and LB methods give rise to an evolution of the ionic concentrations and fluid velocity satisfying the coupled Poisson-Nernst-Planck and Navier-Stokes equations (1)–(3).

C. Imposing conducting boundary conditions

The Poisson equation (2) must be solved numerically at each time step to determine the electrostatic potential $\psi(\mathbf{r})$ from the charge distribution ρ_{el} on the lattice. Following previous implementations of the LBE algorithm, we use the Successive Over Relaxation (SOR) method,^{48,49,56} which we modify as described below to impose constant-potential boundary conditions and to determine the charged induced at the surface of the metal. Introducing the reduced potential $\phi(\mathbf{r}) = \beta e \psi(\mathbf{r})$, the Poisson equation can be rewritten as $\nabla^2 \phi + 4\pi l_B \frac{\rho_{el}}{e} = 0$. Then, we discretize the Laplacian using a stencil consistent with the LB lattice, which can be derived from the

Taylor expansion: $\phi(\mathbf{r} + \mathbf{c}_i \Delta t) \approx \phi(\mathbf{r}) + \Delta t \nabla \phi \cdot \mathbf{c}_i + \frac{\Delta t^2}{2} \nabla \nabla \phi : \mathbf{c}_i \mathbf{c}_i$. Using the sum rules for the lattice, $\sum_i w_i = 1$, $\sum_i w_i c_{i\alpha} = 0$, and $\sum_i w_i c_{i\alpha} c_{i\beta} = c_s^2 \delta_{\alpha\beta}$, where $\delta_{\alpha\beta}$ is the Kronecker symbol (1 if $\alpha = \beta$, 0 otherwise) and $\{\alpha, \beta\} \in \{x, y, z\}$ refer to the components of the discrete velocities, it then follows that the Laplacian can be approximated by

$$\nabla^2 \phi(\mathbf{r}) = \frac{2}{c_s^2 \Delta t^2} \sum_i w_i [\phi(\mathbf{r} + \mathbf{c}_i \Delta t) - \phi(\mathbf{r})]. \quad (12)$$

In practice, starting from an initial guess of the potential (e.g., uniform at $t = 0$ or from the potential at the previous time step), the potential is found iteratively according to

$$\phi_{h+1}(\mathbf{r}) = \phi_h(\mathbf{r}) + \omega \frac{c_s^2 \Delta t^2}{2} \left[\nabla^2 \phi_h(\mathbf{r}) + 4\pi l_B \frac{\rho_{el}(\mathbf{r})}{e} \right] \quad (13)$$

with ω being a constant (here 1.4) chosen to ensure numerical stability and convergence as a function of iteration h . It is straightforward to see that if convergent, the procedure yields a solution of the Poisson equation. Compared to LB-based methods with a fictitious dynamics for the potential with a prescribed (large) number of iterations at each LB step, in the present approach, the procedure stops once convergence is reached (this can be achieved within a few iterations when starting from the solution at the previous LB step).

Up to now, this procedure has been used successfully with charged colloids or charged porous media in which the charge density of the solid is known. Note that, in general, the distribution of the charge within the solid (e.g., localized at the interface or homogeneously) matters if one wants to model solids with a fixed surface charge density.⁵⁸ In the present work, our interest goes instead to model metallic solids with fixed potential. The simplest solution is to update the potential as described above in the liquid while maintaining the potential of the solid nodes at the prescribed values ψ_s . This is possible, but the results on the liquid side are only accurate to first order in the lattice spacing Δx . Indeed, as mentioned, the location of the physical interface between the solid and the liquid lies at the midplane between the solid and liquid nodes, not on the last layer of solid nodes (the situation is more complex on curved boundaries).

In order to be consistent with this observation, we therefore propose a slightly modified algorithm: For each boundary link, i.e., such that \mathbf{r} and $\mathbf{r} + \mathbf{c}_i \Delta t$ belong to different phases (interfacial nodes), we simply multiply by 2 the difference appearing in Eq. (12) when computing the Laplacian in Eq. (13) (in order to determine the potential on interfacial liquid nodes). The fact that this effectively places the boundary condition at the midplane is illustrated in Fig. 1 in the case of a one-dimensional geometry. A related discussion can be found in Ref. 41, where the ion dynamics was simulated using finite elements [see their Eq. (15) and below]. The proposed modification applies this idea to the stencils used for differential operators consistent with the LB lattice (for a discussion of stencils in the bulk, see Ref. 59). It proves convenient to reformulate the modification in a compact form by introducing the characteristic function of the solid,

$$\chi_s(\mathbf{r}) = \begin{cases} 1 & \text{if } \mathbf{r} \text{ is a solid node,} \\ 0 & \text{if } \mathbf{r} \text{ is a fluid node.} \end{cases} \quad (14)$$

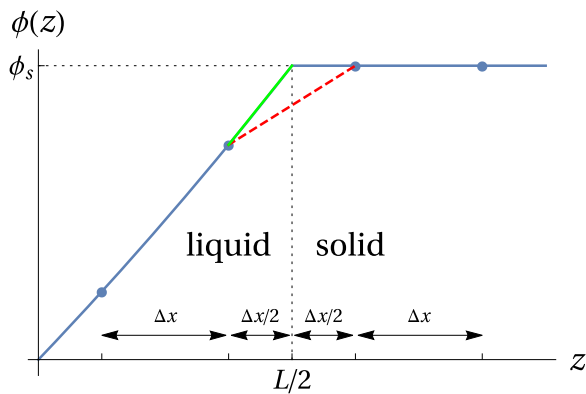


FIG. 1. Enforcing the constant potential boundary condition (Dirichlet). The electrostatic potential is displayed as a function of position, in the vicinity of a solid electrode. For consistency with the hydrodynamic treatment, the liquid-solid interface is located halfway between two lattice nodes, as illustrated by the vertical dotted line at $z = L/2$. The resolution is Δx and the reduced potential of the electrode is fixed at a constant value ϕ_s . The ratio between the slopes of the thick (green) and dashed (red) lines is two. Unlike the former, the latter provides a poor estimation of the gradient at the interface, as illustrated by the figure. A consistent calculation of the gradient at the interface requires to account for this factor of two, which, in turn, leads to the modified Laplacian in Eq. (15) as compared to Eq. (12). While ϕ is prescribed in the solid region, the Poisson equation is solved in the liquid side.

Equation (12) is then replaced by

$$\nabla^2 \phi(\mathbf{r}) = \frac{2}{c_s^2 \Delta t^2} \sum_i w_i [\phi(\mathbf{r} + \mathbf{c}_i \Delta t) - \phi(\mathbf{r})] [1 + \chi_s(\mathbf{r} + \mathbf{c}_i \Delta t) - \chi_s(\mathbf{r})] \quad (15)$$

when solving the Poisson equation via Eq. (13). A *bona fide* feature of this reformulation is that it is parametrization independent and can be used for arbitrary geometry of the solid electrode. Note that this introduces a correction [with respect to Eq. (12)] only at the boundaries, which can be shown using the above-mentioned Taylor expansion and sum rules to correspond to a surface term $2\nabla\phi(\mathbf{r}) \cdot \nabla\chi_s(\mathbf{r}) = -\frac{\sigma}{\epsilon_0 \epsilon_r} \mathbf{n}$, with σ being the local surface charge density and \mathbf{n}

being the local normal unit vector pointing out of the electrode (the factor of 2 again corresponds to the location of the interface between the solid and liquid nodes, as sketched in Fig. 1).

Once the potential distribution inside the liquid is known, in particular, at the interfacial liquid nodes, we can compute the charge Q of the electrodes using again the Poisson equation as

$$Q = \Delta x^3 \sum_{\mathbf{r} \in \text{elec}} \rho_{el}(\mathbf{r}) = -\frac{e \Delta x^3}{4\pi l_B} \sum_{\mathbf{r} \in \text{elec}} \nabla^2 \phi(\mathbf{r}), \quad (16)$$

where the Laplacian is computed via Eq. (15) and vanishes everywhere inside the electrode except at interfacial nodes, as expected for the charge induced by the polarization of a metal.

We will show in Sec. III that the method presented in this section allows us to recover the correct potential throughout the liquid and in turn the correct ionic density profiles at steady-state, as well as the corresponding capacitance of the electrode with second order accuracy in the lattice spacing. As for the rest of the link-flux method, the discretization of the differential operators is only accurate for sufficiently small variations of the considered quantities between neighboring nodes, e.g., for the potential: $\beta e |\psi(\mathbf{r} + \mathbf{c}_i \Delta t) - \psi(\mathbf{r})| \ll 1$. This, in turn, indicates how small the lattice spacing should be (as *a priori* guess to setup the simulation and as *a posteriori* validity check). We underline, however, that the voltage between electrodes need not be small and that nonlinear electrostatic regimes can be simulated using the present method provided that the lattice spacing is well chosen. Since larger gradients are expected in nonlinear regimes, one can anticipate that smaller lattice spacings are necessary in that case.

III. RESULTS AND DISCUSSION

In the following, we validate our approach to impose constant-potential boundary conditions in LBE simulations by considering cases for which it is possible to obtain analytical results, in the linear regime. However, the method can also be readily applied without this restriction. We consider two geometries, illustrated in Fig. 2, corresponding to parallel plate and cylindrical (coaxial) capacitors, with a 1:1 electrolyte ($z_+ = -z_- = 1$) at concentration ρ_s corresponding to a Debye screening length $\lambda_D = (8\pi l_B \rho_s)^{-1/2}$. We assume for simplicity that both cations and anions have the same diffusion

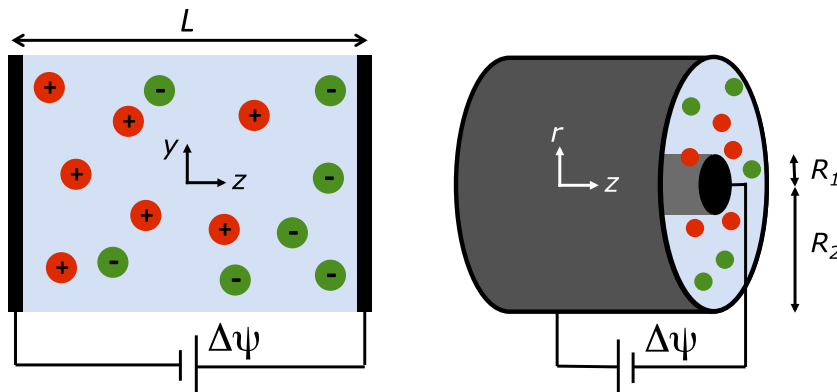


FIG. 2. Capacitors consisting of an electrolyte confined between two metallic electrodes maintained at a constant potential difference $\Delta\psi$. Two geometries are considered: parallel plate capacitor (left) with electrodes separated by a distance L , and coaxial capacitor (right) with electrodes of inner and outer radii R_1 and R_2 . In the following, we also consider the electro-osmotic flow induced in the charged capacitors by an additional electric field in the y (respectively, z) direction for the parallel plate (respectively, coaxial) capacitor.

coefficient $D_+ = D_- = D$, but the simulations can be readily performed without this restriction.

A. Parallel plate capacitor

We first consider parallel plate capacitors with two planar electrodes separated by a distance L (in the z direction, with $z = 0$ at the midplane). Starting from an uncharged capacitor, we apply at $t = 0$ a voltage $\Delta\psi = \psi_2 - \psi_1 = 2.5$ mV between the two electrodes, or in reduced units (in terms of the thermal voltage $k_B T/e \approx 25$ mV): $\beta e \Delta\psi = 0.1$. With such a small reduced voltage, it is possible to linearize the Poisson-Nernst-Planck equation to obtain the time-dependent charge on the positive electrode $Q(t)$ as well as the steady-state potential and ionic density profiles in the capacitor, which corresponds to the Debye-Hückel (DH) theory.

LBE simulations in this geometry are performed for a system with periodic boundary conditions in all directions, with $N_x = N_y = 1$ lattice nodes in the directions parallel to the surfaces (this is sufficient to simulate infinite planar walls, as we checked by also performing simulations for $N_x = N_y = 3$ for one of the systems). In the direction perpendicular to the electrodes, we use $N_z = N_f + 6$ nodes, where $N_f = L/\Delta x$ (with L being the distance between the solid/liquid interfaces and Δx being the lattice spacing) is the number of layers of fluid nodes, and 3 layers of nodes on each side of the liquid for the two electrodes. This choice ensures that there is no effect of the periodic boundary conditions in this direction on the charge induced at the surface of each electrode. We use a BGK relaxation $\tau = \Delta t$, which corresponds to a kinematic viscosity of $\nu = \frac{\eta}{\rho} = \frac{1}{6} \frac{\Delta x^2}{\Delta t}$. The diffusion coefficient of the ions is taken as $0.05 \frac{\Delta x^2}{\Delta t}$, to ensure that the Schmidt number $Sc = \nu/D$ is larger than one, as for small ions in water (even though the order of magnitude is larger in this case). The potentials of the two electrodes are arbitrarily chosen as $\psi_1 = 0.1 k_B T/e$ and $\psi_2 = 0.2 k_B T/e$ to apply the desired voltage, but the resulting evolution of the ionic densities and electrode charge do not depend on the absolute potentials, as expected.

1. Potential and concentration profiles

Before examining the charge induced on the electrodes and the corresponding capacitance, we first examine the potential and concentration profiles through the capacitor, which are reported in Fig. 3 for simulation parameters indicated in its caption. As explained above, the initial potential profile corresponds to the solution of the Poisson equation for a neutral capacitor, since the charge density vanishes inside the liquid because $\rho_+(z) = \rho_-(z) = \rho_s$ everywhere before the ions start moving. The corresponding initial electric field drives the cations and anions toward opposite electrodes. Once the electric double layers are established, there is no field in the bulk part of the liquid, i.e., at distances much larger than λ_D (this can be achieved only in the regime $\lambda_D \ll L$).

The solution of the DH equation (5) for the parallel plate capacitor with boundary conditions $\psi(+L/2) = \psi_2$ and $\psi(-L/2) = \psi_1$ is given by

$$\psi^{DH}(z) = \frac{\psi_1 + \psi_2}{2} + \left(\frac{\psi_2 - \psi_1}{2} \right) \times \frac{\sinh(\kappa z)}{\sinh(\kappa L/2)}. \quad (17)$$

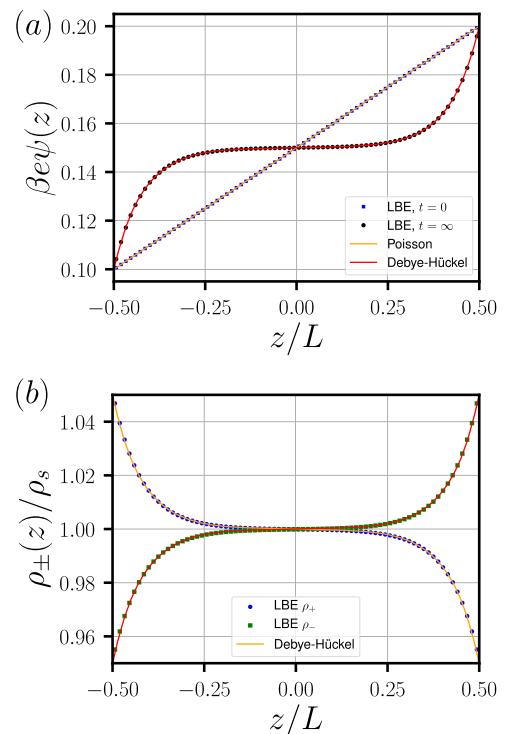


FIG. 3. Steady-state electrostatic potential ψ (a) and ionic concentration ρ_{\pm} (b) profiles in a parallel plate capacitor, obtained from Lattice Boltzmann electrokinetics simulations (LBE, symbols) and Debye-Hückel theory (lines). Results are normalized by the thermal potential $k_B T/e$ and salt concentration ρ_s , respectively. In panel (a), we also indicate the initial potential profile: Right after establishing the potential drop and before the ions start to move, the fluid is neutral and the solution of the Poisson equation in this geometry is linear, as for a simple dielectric parallel plate capacitor. Simulations are performed for a separation $L = 76\Delta x$, with a lattice spacing $\Delta x = l_B/1.44$, with l_B being the Bjerrum length, a salt concentration corresponding to a Debye length $\lambda_D = 6\Delta x$, and a reduced voltage $\beta e \Delta\psi = 0.1$.

Therefore, in the steady-state regime and the small voltage limit, both the potential and ionic density profiles decay exponentially from the surface, with a decay length λ_D . The LBE results are in excellent agreement with these analytical predictions in the considered range of physical and simulation parameters [which are the same as for Fig. 4(a)]. This is a first validation of the proposed method to impose the fixed potential boundary conditions.

2. Charge and capacitance

As explained in Sec. II C, we can compute the instantaneous charge $Q(t)$ on the electrode surface from the potential distribution (once it has been determined from the ionic concentration via the Poisson equation) using Eq. (16). Figure 4(a) shows the charge as a function of time for a capacitor with electrodes separated by a distance $L \approx 52.8 l_B \approx 36.9$ nm and electrolyte concentration (0.011 mol l^{-1}) such that $\lambda_D \approx 4.2 l_B \approx 2.9$ nm. The simulation parameters are indicated in the caption of Fig. 4. The charge is reported normalized by the DH prediction for the surface capacitance,

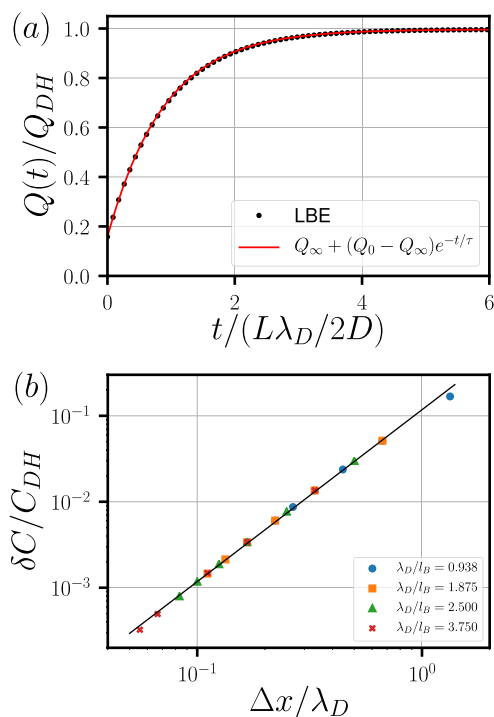


FIG. 4. (a) Charging a parallel plate capacitor: The charge obtained from lattice Boltzmann electrokinetics (LBE) simulations, normalized by the Debye-Hückel prediction for the surface capacitance $C_{DH} = \epsilon_0 \epsilon_r / 2\lambda_D$, as a function of time normalized by $L\lambda_D/2D$. The initial value of the charge coincides with the expected value for a dielectric (neutral) capacitor $C_0 = \epsilon_0 \epsilon_r / L$. Simulations are performed for a separation $L = 76\Delta x$, with a lattice spacing $\Delta x = l_B/1.44$, with l_B being the Bjerrum length, a salt concentration corresponding to a Debye length $\lambda_D = 6\Delta x$, and a reduced voltage $\beta e\Delta\psi = 0.1$. Results are shown only every 400 steps for clarity. The line shows an exponential fit of the LBE results (see Fig. 5 for a discussion of the characteristic times), while horizontal and vertical lines are only guides to the eye. (b) Influence of the lattice spacing. The relative deviation of the simulated capacitance (computed from Q_∞) with respect to the Debye-Hückel prediction is reported as a function of the ratio $\Delta x/\lambda_D$, for several salt concentrations corresponding to different ratios λ_D/l_B and a fixed ratio $L/l_B = 52.5$. The line has a slope of 2.

$$C_{DH} = \epsilon_0 \epsilon_r / 2\lambda_D, \quad (18)$$

which can be interpreted physically as the capacitance for two parallel plate capacitors with distance λ_D in series. Time is normalized by $L\lambda_D/2D$. The results well converge to the DH prediction, which is expected to be valid for such a small voltage and takes the form of Eq. (18) when $\lambda_D \ll L$. The charging dynamics will be analyzed in more detail in Sec. III A 3, but one can already note the exponential form of the charge as a function of time, illustrated by the solid line. Another point of interest is the initial value of the charge, which does not vanish once voltage is applied, but rather corresponds to the value for a dielectric (neutral) capacitor: $C_0 = \epsilon_0 \epsilon_r / L$. This is due to the fact that the liquid is neutral before the ions start moving [see the potential distribution inside the liquid in Fig. 3(a)].

Of course, the accuracy of the simulation results depends on the level of discretization, more specifically the grid spacing Δx with

respect to the physical lengths. The latter are generally in the order $l_B < \lambda_D < L$, even though the order of the last two can be reversed for small electrolyte concentrations and distances between electrodes. The grid spacing must be sufficiently small to resolve the electric double layers at steady-state ($\Delta x/\lambda_D < 1$).

Figure 4(b) shows the relative error on the steady-state capacitance with respect to the DH result as a function of $\Delta x/\lambda_D$, for a fixed ratio $L/l_B = 52.5$ and several values of λ_D/l_B (changing the lattice spacing Δx also changes the time step Δt when working, as we do here, with constant viscosity and diffusion coefficients in reduced units $\Delta x^2/\Delta t$, but this has no influence on the steady-state capacitance). The slope of 2 on this double logarithmic scale indicates that

$$\frac{|C_{LBE} - C_{DH}|}{C_{DH}} \propto \left(\frac{\Delta x}{\lambda_D}\right)^2, \quad (19)$$

for all considered cases, i.e., our algorithm to impose constant-potential boundary conditions and to determine the surface charge induced by the ionic distributions in the electrolyte is accurate to second order. Note that we have pushed the numerical results to the rather extreme case of $\lambda_D \approx l_B$: this is a high concentration regime in which the DH theory itself becomes too crude an approximation because correlations between ions (in particular, due to the excluded volume) cannot be neglected.

3. Charging dynamics

The LBE simulations do not only provide the steady-state electrode charge and potential/concentration profiles but also their evolution with time. Figure 5(a) reports simulation results for the electrode charge similar to those of Fig. 4(a), at a fixed salt concentration (0.065 mol l^{-1} , corresponding to $\lambda_D = 1.2 \text{ nm}$) and resolution ($\Delta x/l_B$) but for several distances between electrodes L (see the caption for details) and in a scale that emphasizes the exponential relaxation of $Q(t)$ toward the steady-state solution. This scale clearly shows that the corresponding characteristic time (inverse of the slope) depends on the system.

As pointed out, e.g., by Bazant and co-workers,²⁰ the decay time is neither the Debye relaxation time λ_D^2/D (which is the relaxation time for bulk electrolytes) corresponding to diffusion over the Debye length nor the diffusion time over the distance L between the electrodes, but rather $\sim L\lambda_D/2D$. More accurate analytical expressions have been derived in Ref. 20 and more recently by Janssen and Bier in Ref. 21, which include a correction of order λ_D^2/D . The result can be interpreted as an RC charging time taking into account the capacitance of the electrode-electrolyte interfaces, estimated by C_{DH} , and the resistance of the bulk electrolyte, using the conductivity estimated via the Nernst-Einstein expression and considering a slab of width $\approx L - \lambda_D$ of the electrolyte. The characteristic decay time τ is reported in Fig. 5(b), normalized by $L\lambda_D/2D$, as a function of the ratio $2\lambda_D/L$. The results are in perfect agreement with the results of Ref. 21, which also coincide with those of Ref. 20 for $\lambda_D \ll L$.

4. Electrokinetic effects

Finally, the LBE method is able to capture the electrokinetic coupling between the ions and the solvent. This is illustrated in the present case of constant-potential walls by examining the

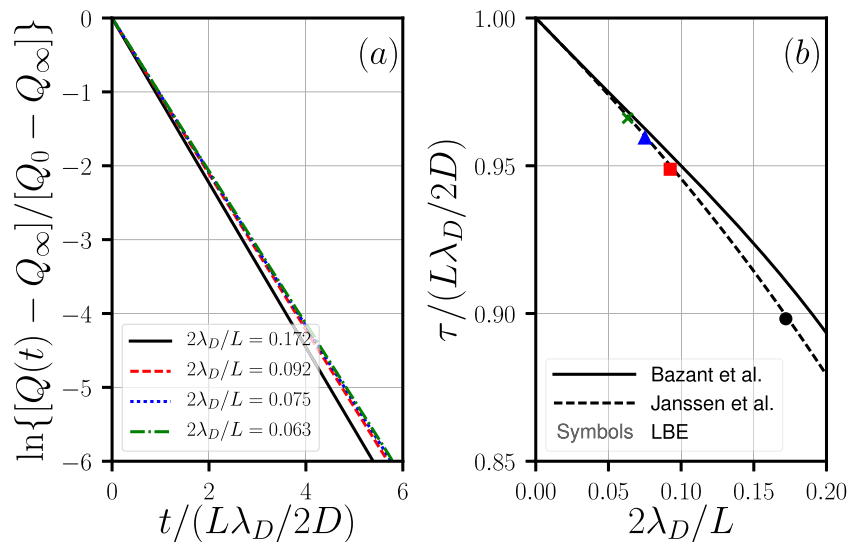


FIG. 5. Charging dynamics in parallel plate capacitors. (a) Relaxation of the charge of the electrode $Q(t)$ from its initial value Q_0 to its final value Q_∞ , plotted on a logarithmic scale to illustrate the exponential decay, which allows us to define a relaxation time τ . (b) Relaxation time, normalized by the characteristic time $L\lambda_D/2D$, as a function of the ratio between the Debye screening length and the half-distance between the electrodes. Simulations (symbols) are performed for several interelectrode distances L , corresponding to the colors indicated in panel (a), with a lattice spacing $\Delta x = l_B/4.8$, with l_B being the Bjerrum length, a salt concentration corresponding to a Debye length $\lambda_D = 8\Delta x$, and a reduced voltage $\beta e\Delta\psi = 0.1$. The relaxation time for each L is reported in panel (b) with the corresponding color. The simulation results are also compared to the analytical predictions in Eq. (36) of Ref. 20 and in Eq. (29) and preceding definitions of Ref. 21.

electro-osmotic response of the *charged* parallel plate capacitor (obtained as the steady-state of Secs. III A 1–III A 3) to an additional electric field E_y parallel to the electrodes. Note that in a real system of a capacitor with finite lateral dimensions, such an additional field would be applied by other electrodes, located outside of the capacitor, and the field lines would be modified compared to the simplified case considered here for validation purposes. For a sufficiently small applied field, the electro-osmotic flow is laminar and the steady-state solution of the Navier-Stokes equation (3) in this geometry, with no-slip boundary conditions and in the Debye-Hückel limit, is given by

$$u_y(z) = \frac{\varepsilon_0 \varepsilon_r E_y (\psi_2 - \psi_1)}{\eta} \times \frac{1}{2} \left(\frac{\sinh(\kappa z)}{\sinh(\kappa L/2)} - \frac{2z}{L} \right). \quad (20)$$

Figure 6 reports the simulation results corresponding to the system already shown in Fig. 3 with an applied electric field in the y direction of magnitude $\beta e E_y \Delta x = 0.01$. It perfectly reproduces the analytical result expected to be valid for the considered range of physical parameters, which confirms the validity of the LBE scheme. We note that the resulting flow profile corresponds to shearing the fluid by applying opposite forces in the two double layers (since they are oppositely charged). This differs from the common situation of shear induced by moving walls in opposite directions, since the electrodes are not mobile in the present case.

Figure 6 also shows electro-osmotic flow profiles in the transient regime. The flow builds up in the electric double layers near the electrodes and develops by momentum diffusion in the direction perpendicular to the electrodes, over a characteristic time scale

$\tau_v = L^2/\pi^2\nu$ with $\nu = \eta/\rho$ being the kinematic viscosity of the fluid.

As a final remark on the parallel plate capacitor, we emphasize again that the comparison is made here only in the linear regime

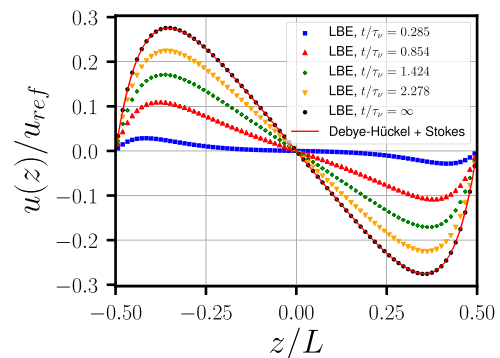


FIG. 6. Electro-osmotic flow profile in a charged parallel plate capacitor, in the presence of an additional electric field E_y along the electrodes. The situation at $t = 0$ corresponds to the steady state of the charged capacitor. Lattice Boltzmann Electrokinetics (LBE) simulations are shown with the symbols. The steady-state profile is compared to the theoretical result [Eq. (20)] combining Debye-Hückel theory for the electrostatic potential and the Stokes equation for the flow (line). Results are scaled with the reference velocity $u_{ref} = \varepsilon_0 \varepsilon_r E_y (\psi_2 - \psi_1)/\eta$. Simulations are performed under the same conditions as in Fig. 3, with a reduced applied field $\beta e E_y \Delta x = 0.01$ parallel to the electrodes. The LBE simulations provide the time-dependence of the electrokinetic response, which reaches steady-state over a time scale $\tau_v = L^2/\pi^2\nu$ with $\nu = \eta/\rho$ being the kinematic viscosity of the fluid, as expected from the momentum diffusion in the direction perpendicular to the flow.

where DH theory applies for validation purposes, but that the LBE simulations would provide the numerical solution of the nonlinear PNP and Navier-Stokes outside of this regime.

B. Cylindrical (coaxial) capacitor

The setup to simulate cylindrical capacitors is illustrated in Fig. 7. As for the parallel plates geometry, periodic boundary conditions along z , in principle, allow us to use a single lattice node in this direction to simulate an infinite system.

1. Potential profile

As for the parallel plate capacitor, we first examine the initial and steady-state potential profiles within the electrolyte. LBE simulations were performed in the setup illustrated in Fig. 7, with a grid of $N_x \times N_y \times N_z = 74 \times 74 \times 3$ nodes, a lattice spacing $\Delta x = l_B/1.2$, inner and outer cylinder radii of $R_1 = 2\Delta x \approx 1.2$ nm and $R_2 = 35\Delta x \approx 20.4$ nm, respectively, and a salt concentration (≈ 0.0034 mol l^{-1}) corresponding to a screening length $\lambda_D = 9\Delta x = 7.5l_B \approx 5.25$ nm. With this choice of the box size and outer radii, the width of the outer electrode region is $w = 4\Delta x$ (see Fig. 7).

The potential satisfies the Poisson equation (2), with boundary conditions $\psi(R_1) = \psi_1$ and $\psi(R_2) = \psi_2$ as well as the constraint of opposite surface charge of the two cylinders leading to $R_1\psi'(R_1) = R_2\psi'(R_2)$. Before the ions start moving ($t = 0$), the solution reads

$$\psi_0^{cyl}(r) = \psi_1 + (\psi_2 - \psi_1) \frac{\ln(r/R_1)}{\ln(R_2/R_1)}, \quad (21)$$

with r being the radial distance from the axis of both cylindrical electrodes. Figure 8 shows that the initial potential profile obtained numerically with the SOR algorithm is in excellent agreement with this analytical solution, even though the inner cylinder is discretized quite roughly ($R_1 = 2\Delta x$ only). This further demonstrates the

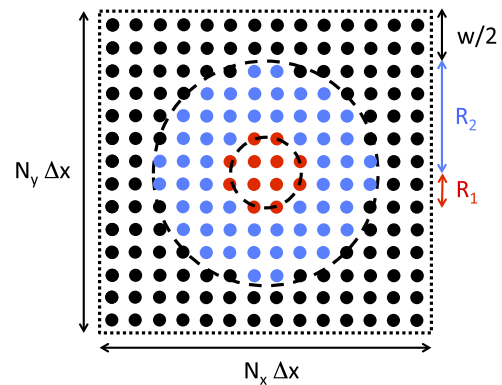


FIG. 7. Simulation setup for the coaxial capacitor. The lattice consists of $N_x \times N_y \times N_z$ nodes with periodic boundary conditions in all directions (here a cut in the xy plane is shown) at the boundaries of the box shown in dotted lines. The nodes corresponding to the fluid region, illustrated in blue, are located between two cylinders of radii R_1 (inner electrode, in red) and R_2 (outer electrode, in black) with potentials ψ_1 and ψ_2 , respectively. All the region beyond the outer cylinder is maintained at the same potential (this defines the width w of the electrode region as shown in the figure).

accuracy of our numerical scheme to impose constant-potential boundary conditions in a more complex geometry than the planar electrodes.

Figure 8 also compares the LBE simulation results for the steady-state potential profile with the analytical solution of the DH equation (5) given by⁶⁰

$$\psi_{DH}^{cyl}(r) = \psi_1 + (\psi_2 - \psi_1) f(r, R_1, R_2, \kappa) \quad (22)$$

with

$$f(r, R_1, R_2, \kappa) = \frac{[R_2 K_1(\kappa R_2) - R_1 K_1(\kappa R_1)][I_0(\kappa r) - I_0(\kappa R_1)] + [R_2 I_1(\kappa R_2) - R_1 I_1(\kappa R_1)][K_0(\kappa r) - K_0(\kappa R_1)]}{[R_2 K_1(\kappa R_2) - R_1 K_1(\kappa R_1)][I_0(\kappa R_2) - I_0(\kappa R_1)] + [R_2 I_1(\kappa R_2) - R_1 I_1(\kappa R_1)][K_0(\kappa R_2) - K_0(\kappa R_1)]}, \quad (23)$$

where I_α and K_α are the modified Bessel functions of the first and second kind. The LBE results are again in excellent agreement with the analytical DH predictions, which are expected to be valid in this low-voltage regime.

2. Capacitance

We now turn again to the charge induced on the electrode and the corresponding capacitance. The electrode charge per unit length is conveniently derived using the Gauss theorem from the electric field at the surface of the electrodes. Taking derivatives of the potential with respect to voltage $\psi_2 - \psi_1$ and to the radial distance r (evaluated at $r = R_1$), it follows from Eqs. (21)–(23) that the capacitances per unit length are $C_0^{cyl} = 2\pi\epsilon_0\epsilon_r/\ln(R_2/R_1)$ for a neutral

liquid (before the ions start moving) and

$$C_{DH}^{cyl} = 2\pi\epsilon_0\epsilon_r R_1 f'(R_1, R_1, R_2, \kappa) \quad (24)$$

at steady-state (within the Debye-Hückel limit).

LBE simulations were performed in the setup illustrated in Fig. 7, with a grid of $N_x \times N_y \times N_z = 54 \times 54 \times 3$ node, with inner and outer cylinder radii of $R_1 = 2\Delta x$ and $R_2 = 25\Delta x$, respectively, and with a lattice spacing $\Delta x = l_B/1.2$. The reduced potential difference is again fixed to $\beta e\Delta\psi = 0.1$, and the concentration is varied over a range corresponding to $\lambda_D/\Delta x = 3, 6, 9$, and 12.

Table I reports the relative errors for the capacitance computed at steady-state in the LBE simulations with respect to the Debye-Hückel analytical result [Eq. (24)] which is expected to be

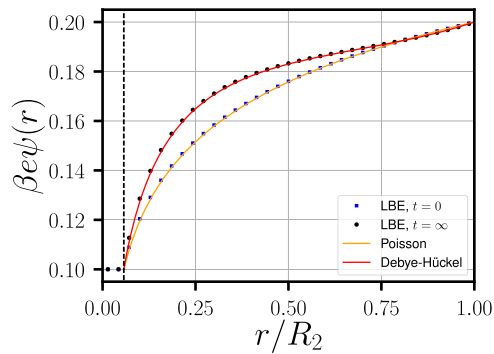


FIG. 8. Electrostatic potential profile in a coaxial cylindrical channel, obtained from lattice Boltzmann electrokinetics simulations (LBE, symbols) and Debye-Hückel theory (line). We also indicate the initial potential profile: Before the ions start to move, the fluid is neutral and the solution of the Poisson equation in this geometry is the same as the one for a simple dielectric coaxial capacitor [see Eq. (21)]. Simulations are performed for an inner radius $R_1 = 2\Delta x$ and an outer radius $R_2 = 35\Delta x$, with a lattice spacing $\Delta x = l_B/1.2$, with l_B being the Bjerrum length, a salt concentration corresponding to a Debye length $\lambda_D = 9\Delta x$, and a reduced voltage $\beta e\Delta\psi = 0.1$ between the inner and outer electrodes. The vertical dashed line indicates the location of the interface on the inner cylinder.

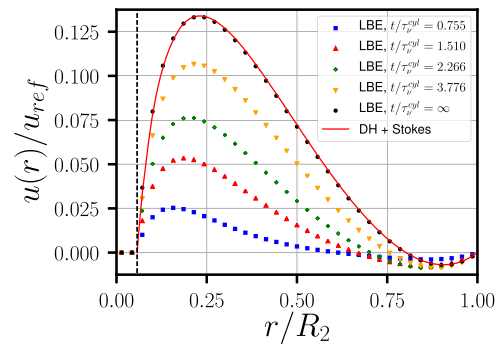


FIG. 9. Electro-osmotic flow profile in a coaxial capacitor, in the presence of an additional electric field E_z along the electrodes. The situation at $t = 0$ corresponds to the steady state of the charged capacitor. Lattice Boltzmann electrokinetics simulations (LBE, symbols) for the steady-state are compared to the theoretical result Eq. (25) combining Debye-Hückel theory for the electrostatic potential and the Stokes equation for the flow (line). Results are scaled with the reference velocity $u_{ref} = \varepsilon_0 \varepsilon_r E_z (\psi_2 - \psi_1) / \eta$. Simulations are performed under the same conditions as in Fig. 8, with a reduced applied field $\beta e E_z \Delta x = 0.0001$ parallel to the electrodes. The LBE simulations further provide the time-dependence of the electrokinetic response, which reaches steady-state over a time scale $\tau_v^{st} = (R_2 - R_1)^2 / \pi^2 \nu$.⁶¹ The vertical dashed line indicates the location of the interface on the inner cylinder.

valid in this low-voltage regime. The errors are very small for the chosen range of simulation parameters. Similar to the slit case, the error decreases as $(\Delta x / \lambda_D)^2$ when the resolution of the double layer increases. However, the extrapolated value for $\Delta x / \lambda_D \rightarrow 0$ does not vanish in that case: This residual value ($\sim 0.8\%$) reflects other sources of errors, in particular, due to the coarse discretization of the inner cylinder with a radius of only $R_1 = 2\Delta x$.

3. Electrokinetic effects

We finally examine the electrokinetic response of the charged coaxial capacitor to an additional electric field in the axial z direction. The steady-state electro-osmotic flow profile can be derived from the Stokes equation using the steady-state potential profile, in the Debye-Hückel limit. The result for no-slip boundary conditions at the surface of the electrodes reads

$$u_z(r) = \frac{\varepsilon_0 \varepsilon_r E_z (\psi_2 - \psi_1)}{\eta} \left[f(r, R_1, R_2, \kappa) - \frac{\ln(r/R_1)}{\ln(R_2/R_1)} \right] \quad (25)$$

with f given by Eq. (23).

We performed LBE simulations with the same parameters as described in Sec. III B 1 for the potential profile. Starting from the charged capacitor, we apply a reduced electric field $\beta e E_z \Delta x = 0.0001$ parallel to the electrodes (axial direction z) and monitor

TABLE I. Relative error on the capacitance, computed at steady-state, with respect to the theoretical result [Eq. (24)] in the Debye-Hückel limit, for a coaxial capacitor (see text for simulation details).

$\lambda_D / \Delta x$	3	6	9	12
$ C_{LBE} - C_{DH}^{cyl} / C_{DH}^{cyl}$	2.3%	1.2%	1.0%	0.94%

the velocity of the fluid in this direction, as a function of radial position r and time t . The results shown in Fig. 9 demonstrate that the steady-state velocity profile is in excellent agreement with the analytical result Eq. (25), as a last illustration of the validity of the proposed method to impose constant-potential boundary conditions. The transient regime (for which no analytical result is available) is consistent with the expected acceleration near the electrode surfaces, where the fluid is not neutral, followed by viscous momentum diffusion away from these regions to the whole fluid with a characteristic time $\propto (R_2 - R_1)^2 / \nu$.⁶¹

As for the parallel plate capacitor, we note that the steady state corresponds to shearing the fluid via opposite forces within the two double layers. This results, in particular, in flows in opposite directions near the two electrodes, but with very different magnitudes in that case (larger velocity near the inner electrode) since the total fluid flux vanishes (there is no net force on the fluid which is overall neutral). Such an original setup may find applications to separate species in a mixture of ions.

IV. CONCLUSION

We have introduced a simple rule to impose Dirichlet electrostatic boundary conditions in LBE simulations in a consistent way with the location of the hydrodynamic interface (for stick boundary conditions), i.e., between the solid and liquid nodes rather than on the solid nodes. The proposed method also provides the instantaneous local charge induced on the electrode by the instantaneous distribution of ions under voltage. We validated it in the low voltage regime by comparison with analytical results in two model capacitors (parallel plate and coaxial electrodes), examining the steady-state ionic concentrations and electric potential profiles, the time-dependent response of the charge on the electrodes, and the

steady-state electro-osmotic profiles in the presence of an additional, tangential electric field. The LBE method naturally provides the time-dependence of all these quantities—a possibility that we illustrate on the electro-osmotic response. Compared to the direct numerical solution of the macroscopic transport equations (Poisson-Nernst-Planck and Navier-Stokes), e.g., via finite differences or finite element methods,^{20,62–64} the LBE approach offers a statistical interpretation which can be exploited to compute other properties such as velocity auto-correlation functions via moment propagation. It also inherits the advantages of the plain LB method for massive parallelization and the simulation of complex geometries (e.g., from an experimental 3D structure of a porous material).

While we do not consider this case in the present work, which focuses on the validation of the method, the latter readily applies to large voltages between the electrodes (not shown), as well as to time-dependent voltages. The only restriction is a sufficiently small lattice spacing, ensuring small variations of the considered quantities between neighboring nodes, in particular, small potential differences compared to $k_B T/e$. Besides, we have shown that the method is accurate to second order in lattice spacing. If necessary, the numerical stability and accuracy of the algorithm can be improved straightforwardly using the approaches already introduced for the LBE method, such as using a multiple relaxation time (or simply two relaxation time, as done in Refs. 54 and 55) kernel for the evolution of LB populations, or a multiple-time step approach, as described in the original article of Capuani *et al.*,⁴⁹ which allows the simulation of larger diffusion coefficients.

This work opens the way to the LBE simulation of more complex systems involving electrodes and metallic surfaces, such as the nanofluidic channels and nanotubes mentioned in the Introduction, or porous electrodes, since the algorithm can readily be applied to arbitrary geometries. It would also be a convenient tool for the simulation of other electrokinetic phenomena, such as induced-charged electrokinetics.⁶⁵ On the methodological side, possible extensions include the coupling of electrokinetics to adsorption/desorption at the solid-liquid interface,^{66–68} which may play a role in the specific behavior of carbon vs boron nitride nanotubes,⁶⁹ as well as including additional excess terms in the free energy model underlying the present work (which only leads to the emergence of the Nernst-Planck dynamics for the ions). In particular, capturing the effect of ion correlations⁷⁰ would be necessary to simulate more concentrated electrolytes as well as multivalent ions.

ACKNOWLEDGMENTS

The authors are grateful to Lydéric Bocquet and Ignacio Pagonabarraga for useful discussions. A.J.A. and B.R. acknowledge financial support from the French Agence Nationale de la Recherche (ANR) under Grant No. ANR-15-CE09-0013-01. The work was funded by the European Union's Horizon 2020 Research and Innovation Programme under ETN Grant No. 674979-NANOTRANS.

REFERENCES

- X. Blase, L. X. Benedict, E. L. Shirley, and S. G. Louie, "Hybridization effects and metallicity in small radius carbon nanotubes," *Phys. Rev. Lett.* **72**, 1878–1881 (1994).
- L. Rassaei, K. Mathwig, E. D. Goluch, and S. G. Lemay, "Hydrodynamic voltammetry with nanogap electrodes," *J. Phys. Chem. C* **116**, 10913–10916 (2012).
- K. Mathwig and S. G. Lemay, "Pushing the limits of electrical detection of ultralow flows in nanofluidic channels," *Micromachines* **4**, 138–148 (2013).
- S. G. Lemay, S. Kang, K. Mathwig, and P. S. Singh, "Single-molecule electrochemistry: Present status and outlook," *Acc. Chem. Res.* **46**, 369–377 (2013).
- P. Sun and M. V. Mirkin, "Electrochemistry of individual molecules in zeptoliter volumes," *J. Am. Chem. Soc.* **130**, 8241–8250 (2008).
- L. Bocquet and E. Charlaix, "Nanofluidics, from bulk to interfaces," *Chem. Soc. Rev.* **39**, 1073–1095 (2010).
- A. Siria, P. Poncharal, A.-L. Biance, R. Fulcrand, X. Blase, S. T. Purcell, and L. Bocquet, "Giant osmotic energy conversion measured in a single transmembrane boron nitride nanotube," *Nature* **494**, 455–458 (2013).
- E. Secchi, A. Niguès, L. Jubin, A. Siria, and L. Bocquet, "Scaling behavior for ionic transport and its fluctuations in individual carbon nanotubes," *Phys. Rev. Lett.* **116**, 154501 (2016).
- L. Jubin, A. Poggioli, A. Siria, and L. Bocquet, "Dramatic pressure-sensitive ion conduction in conical nanopores," *Proc. Natl. Acad. Sci. U. S. A.* **115**, 4063 (2018).
- G. Gouy, "Sur la constitution de la charge électrique à la surface d'un électrolyte," *J. Phys. Theor. Appl.* **9**, 457 (1910).
- D. Chapman, "A contribution to the theory of electrocapillarity," *Philos. Mag.* **25**, 475 (1913).
- O. Stern, "Zur Theorie der elektrolytischen Doppelschicht," *Z. Elektrochem.* **30**, 508 (1924).
- F. Grün, M. Jardat, P. Turq, and C. Amatore, "Relaxation of the electrical double layer after an electron transfer approached by Brownian dynamics simulation," *J. Chem. Phys.* **120**, 9648–9655 (2004).
- J. I. Siepmann and M. Sprik, "Influence of surface topology and electrostatic potential on water/electrode systems," *J. Chem. Phys.* **102**, 511–524 (1995).
- S. K. Reed, O. J. Lanning, and P. A. Madden, "Electrochemical interface between an ionic liquid and a model metallic electrode," *J. Chem. Phys.* **126**, 084704 (2007).
- C. Merlet, B. Rotenberg, P. A. Madden, and M. Salanne, "Computer simulations of ionic liquids at electrochemical interfaces," *Phys. Chem. Chem. Phys.* **15**, 15781–15792 (2013).
- C. Merlet, C. Péan, B. Rotenberg, P. A. Madden, P. Simon, and M. Salanne, "Simulating supercapacitors: Can we model electrodes as constant charge surfaces?," *J. Phys. Chem. Lett.* **4**, 264–268 (2013).
- D. T. Limmer, C. Merlet, M. Salanne, D. Chandler, P. A. Madden, R. van Roij, and B. Rotenberg, "Charge fluctuations in nanoscale capacitors," *Phys. Rev. Lett.* **111**, 106102 (2013).
- C. Merlet, D. T. Limmer, M. Salanne, R. van Roij, P. A. Madden, D. Chandler, and B. Rotenberg, "The electric double layer has a life of its own," *J. Phys. Chem. C* **118**, 18291–18298 (2014).
- M. Z. Bazant, K. Thornton, and A. Ajdari, "Diffuse-charge dynamics in electrochemical systems," *Phys. Rev. E* **70**, 021506 (2004).
- M. Janssen and M. Bier, "Transient dynamics of electric double layer capacitors: Exact expressions within the Debye-Falkenhagen approximation," *Phys. Rev. E* **97**, 052616 (2018).
- P. M. Biesheuvel and M. Z. Bazant, "Nonlinear dynamics of capacitive charging and desalination by porous electrodes," *Phys. Rev. E* **81**, 031502 (2010).
- L. Joly, C. Ybert, E. Trizac, and L. Bocquet, "Hydrodynamics within the electric double layer on slipping surfaces," *Phys. Rev. Lett.* **93**, 257805 (2004).
- L. Joly, C. Ybert, E. Trizac, and L. Bocquet, "Liquid friction on charged surfaces: From hydrodynamic slippage to electrokinetics," *J. Chem. Phys.* **125**, 204716-1–204716-14 (2006).
- H. Yoshida, H. Mizuno, T. Kinjo, H. Washizu, and J.-L. Barrat, "Molecular dynamics simulation of electrokinetic flow of an aqueous electrolyte solution in nanochannels," *J. Chem. Phys.* **140**, 214701 (2014).
- I. Pagonabarraga, B. Rotenberg, and D. Frenkel, "Recent advances in the modelling and simulation of electrokinetic effects: Bridging the gap between atomistic and macroscopic descriptions," *Phys. Chem. Chem. Phys.* **12**, 9566–9580 (2010).
- B. Rotenberg and I. Pagonabarraga, "Electrokinetics: Insights from simulation on the microscopic scale," *Mol. Phys.* **111**, 827–842 (2013).
- J. Smiattek, M. Sega, C. Holm, U. D. Schiller, and F. Schmid, "Mesoscopic simulations of the counterion-induced electro-osmotic flow: A comparative study," *J. Chem. Phys.* **130**, 244702 (2009).

- ²⁹D. R. Ceratti, A. Obliger, M. Jardat, B. Rotenberg, and V. Dahirel, “Stochastic rotation dynamics simulation of electro-osmosis,” *Mol. Phys.* **113**, 2476–2486 (2015).
- ³⁰V. Dahirel, X. Zhao, B. Couet, G. Batôt, and M. Jardat, “Hydrodynamic interactions between solutes in multiparticle collision dynamics,” *Phys. Rev. E* **98**, 053301 (2018).
- ³¹S. Succi, *The Lattice Boltzmann Equation for Fluid Dynamics and Beyond* (Oxford University Press, 2001).
- ³²V. Lobaskin, B. Dünweg, and C. Holm, “Electrophoretic mobility of a charged colloidal particle: A computer simulation study,” *J. Phys.: Condens. Matter* **16**, S4063 (2004).
- ³³V. Lobaskin, B. Dünweg, M. Medebach, T. Palberg, and C. Holm, “Electrophoresis of colloidal dispersions in the low-salt regime,” *Phys. Rev. Lett.* **98**, 176105 (2007).
- ³⁴O. A. Hickey, C. Holm, J. L. Harden, and G. W. Slater, “Implicit method for simulating electrohydrodynamics of polyelectrolytes,” *Phys. Rev. Lett.* **105**, 148301 (2010).
- ³⁵O. A. Hickey and C. Holm, “Electrophoretic mobility reversal of polyampholytes induced by strong electric fields or confinement,” *J. Chem. Phys.* **138**, 194905 (2013).
- ³⁶A. V. Datar, M. Fyta, U. M. B. Marconi, and S. Melchionna, “Electrokinetic lattice Boltzmann solver coupled to molecular dynamics: Application to polymer translocation,” *Langmuir* **33**, 11635–11645 (2017).
- ³⁷V. Lobaskin and R. R. Netz, “Diffusive-convective transition in the non-equilibrium charging of an electric double layer,” *Europhys. Lett.* **116**, 58001 (2016).
- ³⁸U. M. B. Marconi and S. Melchionna, “Charge transport in nanochannels: A molecular theory,” *Langmuir* **28**, 13727–13740 (2012).
- ³⁹J. Wang, M. Wang, and Z. Li, “Lattice Poisson-Boltzmann simulations of electro-osmotic flows in microchannels,” *J. Colloid Interface Sci.* **296**, 729–736 (2006).
- ⁴⁰V. Thakore and J. J. Hickman, “Charge relaxation dynamics of an electrolytic nanocapacitor,” *J. Phys. Chem. C* **119**, 2121–2132 (2015).
- ⁴¹D. Hlushkou, D. Kandhai, and U. Tallarek, “Coupled lattice-Boltzmann and finite-difference simulation of electroosmosis in microfluidic channels,” *Int. J. Numer. Methods Fluids* **46**, 507–532 (2004).
- ⁴²D. Hlushkou, S. Khirevich, V. Apanasovich, A. Seidel-Morgenstern, and U. Tallarek, “Pore-scale dispersion in electrokinetic flow through a random sphere packing,” *Anal. Chem.* **79**, 113–121 (2007).
- ⁴³D. Hlushkou, K. N. Knust, R. M. Crooks, and U. Tallarek, “Numerical simulation of electrochemical desalination,” *J. Phys.: Condens. Matter* **28**, 194001 (2016).
- ⁴⁴M. Wang and Q. Kang, “Modeling electrokinetic flows in microchannels using coupled lattice Boltzmann methods,” *J. Comput. Phys.* **229**, 728–744 (2010).
- ⁴⁵H. Yoshida, T. Kinjo, and H. Washizu, “Coupled lattice Boltzmann method for simulating electrokinetic flows: A localized scheme for the Nernst-Planck model,” *Commun. Nonlinear Sci. Numer. Simul.* **19**, 3570–3590 (2014).
- ⁴⁶K. Luo, J. Wu, H.-L. Yi, and H.-P. Tan, “Lattice Boltzmann model for Coulomb-driven flows in dielectric liquids,” *Phys. Rev. E* **93**, 023309 (2016).
- ⁴⁷P. B. Warren, “Electroviscous transport problems via lattice-Boltzmann,” *Int. J. Mod. Phys. C* **8**, 889 (1997).
- ⁴⁸J. Horbach and D. Frenkel, “Lattice-Boltzmann method for the simulation of transport phenomena in charged colloids,” *Phys. Rev. E* **64**, 061507 (2001).
- ⁴⁹F. Capuani, I. Pagonabarraga, and D. Frenkel, “Discrete solution of the electrokinetic equations,” *J. Chem. Phys.* **121**, 973–986 (2004).
- ⁵⁰B. Rotenberg, I. Pagonabarraga, and D. Frenkel, “Dispersion of charged tracers in charged porous media,” *Europhys. Lett.* **83**, 34004 (2008).
- ⁵¹I. Pagonabarraga, F. Capuani, and D. Frenkel, “Mesoscopic lattice modeling of electrokinetic phenomena,” *Comput. Phys. Commun.* **169**, 192–196 (2005).
- ⁵²F. Capuani, I. Pagonabarraga, and D. Frenkel, “Lattice-Boltzmann simulation of the sedimentation of charged disks,” *J. Chem. Phys.* **124**, 124903-1–124903-11 (2006).
- ⁵³G. Giupponi and I. Pagonabarraga, “Colloid electrophoresis for strong and weak ion diffusivity,” *Phys. Rev. Lett.* **106**, 248304 (2011).
- ⁵⁴G. Rempfer, G. B. Davies, C. Holm, and J. d. Graaf, “Reducing spurious flow in simulations of electrokinetic phenomena,” *J. Chem. Phys.* **145**, 044901 (2016).
- ⁵⁵M. Kuron, G. Rempfer, F. Schornbaum, M. Bauer, C. Godenschwager, C. Holm, and J. de Graaf, “Moving charged particles in lattice Boltzmann-based electrokinetics,” *J. Chem. Phys.* **145**, 214102 (2016).
- ⁵⁶B. Rotenberg, D. Frenkel, and I. Pagonabarraga, “Coarse-grained simulations of charge, current and flow in heterogeneous media,” *Faraday Discuss.* **144**, 223 (2010).
- ⁵⁷N. Rivas, S. Rijters, I. Pagonabarraga, and J. Harting, “Mesoscopic electrohydrodynamic simulations of binary colloidal suspensions,” *J. Chem. Phys.* **148**, 144101 (2018).
- ⁵⁸A. Obliger, M. Duvaal, M. Jardat, D. Coelho, S. Békri, and B. Rotenberg, “Numerical homogenization of electrokinetic equations in porous media using lattice-Boltzmann simulations,” *Phys. Rev. E* **88**, 013019 (2013).
- ⁵⁹S. P. Thampi, I. Pagonabarraga, and R. Adhikari, “Lattice-Boltzmann-Langevin simulations of binary mixtures,” *Phys. Rev. E* **84**, 046709 (2011).
- ⁶⁰The solution of the Debye-Hückel equation in cylindrical geometry is of the form $\psi_{DH}^{cyl}(r) = aI_0(\kappa r) + bK_0(\kappa r) + c$. The three integration constants a , b , and c are determined by solving the linear system of equations provided by the boundary conditions and constraint of opposite surface charge of the two cylinders, indicated in the text, also using the relations $\frac{dI_0(\kappa r)}{dr} = \kappa I_1(\kappa r)$ and $\frac{dK_0(\kappa r)}{dr} = -\kappa K_1(\kappa r)$.
- ⁶¹The exact expression for the largest momentum relaxation time is $\tau_v^{cyl}/\alpha^2 = (R_2 - R_1)^2/\alpha^2 \pi^2 v$. The value of α is determined by the following equation: $J_0(\frac{\alpha R_1}{R_2 - R_1})Y_0(\frac{\alpha R_2}{R_2 - R_1}) = J_0(\frac{\alpha R_2}{R_2 - R_1})Y_0(\frac{\alpha R_1}{R_2 - R_1})$, where J_0 and Y_0 are the Bessel functions of the first and second kind. Here, α^2 is 0.867 and, in general, a numerical solution of the equation shows that $0.7 < \alpha^2 < 1$.
- ⁶²D. Coelho, M. Shapiro, J. F. Thovert, and P. M. Adler, “Electroosmotic phenomena in porous media,” *J. Colloid Interface Sci.* **181**, 169–190 (1996).
- ⁶³G. Allaire, R. Brizzi, J.-F. Dufreche, A. Mikelic, and A. Piatnitski, “Ion transport in porous media: Derivation of the macroscopic equations using upscaling and properties of the effective coefficients,” *Comput. Geosci.* **17**, 479–495 (2013).
- ⁶⁴G. Pardon and W. van der Wijngaert, “Modeling and simulation of electrostatically gated nanochannels,” *Adv. Colloid Interface Sci.* **199-200**, 78–94 (2013).
- ⁶⁵M. Z. Bazant and T. M. Squires, “Induced-charge electrokinetic phenomena,” *Curr. Opin. Colloid Interface Sci.* **15**, 203–213 (2010).
- ⁶⁶M. Levesque, M. Duvaal, I. Pagonabarraga, D. Frenkel, and B. Rotenberg, “Accounting for adsorption and desorption in lattice Boltzmann simulations,” *Phys. Rev. E* **88**, 013308 (2013).
- ⁶⁷J.-M. Vanson, F.-X. Coudert, B. Rotenberg, M. Levesque, C. Tardivat, M. Klotz, and A. Boutin, “Unexpected coupling between flow and adsorption in porous media,” *Soft Matter* **11**, 6125–6133 (2015).
- ⁶⁸A. Asta, M. Levesque, and B. Rotenberg, “Moment propagation method for the dynamics of charged adsorbing/desorbing species at solid-liquid interfaces,” *Mol. Phys.* **116**, 2965–2976 (2018).
- ⁶⁹B. Grosjean, C. Pean, A. Siria, L. Bocquet, R. Vuilleumier, and M.-L. Bocquet, “Chemisorption of hydroxide on 2D materials from DFT calculations: Graphene versus hexagonal boron nitride,” *J. Phys. Chem. Lett.* **7**, 4695–4700 (2016).
- ⁷⁰B. D. Storey and M. Z. Bazant, “Effects of electrostatic correlations on electrokinetic phenomena,” *Phys. Rev. E* **86**, 056303 (2012).